Research on hybrid topology of single-switch ICPT for battery charging

GUANGZONG ZHANG, CHUNFANG WANG, JIANFEN ZHENG, HOUJI LI

Qingdao University
China
e-mails: zhangguan75@163.com, {qduwcf/jianfenzh}@qdu.edu.cn, lihoushen2008@163.com

Abstract: In order to realize constant current and constant voltage charging for batteries by inductively coupled power transfer (ICPT) technology, a single-switch CL/LCL circuit is designed. The single-switch CL/LCL circuit is composed of a CL/LCL compensation network and single-switch inverter. The proposed circuit is compared with the traditional constant current and constant voltage circuit in the structure. The operating process of the single-switch CL/LCL circuit and the principle to realize a zero-voltage switch (ZVS) are analysed in detail in this paper. The voltage gain and current gain of the circuit are calculated, which demonstrates that the circuit is able to suppress higher harmonics strongly. By using Fourier decomposition, the voltage on the primary-side compensation capacitor can be obtained. After constructing the equivalent mutual inductance model of the circuit, the formulas and parameters are deduced and calculated. Finally, an experiment platform is built to verify the proposed circuit can realize constant current and constant voltage.

Key words: constant current, constant voltage, higher harmonics, ICPT, single-switch inverter

1. Introduction

Inductively coupled power transfer (ICPT) technology has been developing dynamically in recent years. Due to its convenience, safety and other advantages [1, 2], ICPT technology has been widely used to charge batteries of machines in many fields, such as new energy vehicles, mobile phones and unmanned aerial vehicles [3–5].

In order to realize the constant current charging and constant voltage charging of the batteries, some papers have researched the double-side LCCL compensation network of the ICPT

main circuit. Although these high-order compensation networks can deliver constant current and constant voltage, they use too many compensation components, resulting in huge circuit volume and too many unstable factors. The modelling analysis and parameters design methods of a double-side LCCL compensation network are given in [6, 7]. Authors in [7] proposed the compactness of the double-side LCCL system that can be improved by integrating the compensated coils into the main coil structure. This method is limited by the coil structure which is flexible in practical application, and the integration method is complex. The output characteristics of four basic resonant networks are briefly analysed, and a hybrid compensation network is proposed to deliver constant current and constant voltage by switching the primary-side compensation structure in [8]. But three switches are added to the primary-side compensation network, which increases the cost of the circuit. A compensation network is proposed to obtain the constant current and voltage by switching the primary and secondary compensation networks at the same time in [9]. Compared with the double-side LCCL network, the compensation networks in [8] and [9] are simple when the network is working. However, the control methods of the compensation networks in [8] and [9] are complex, because the communication between the primary and secondary sides also needs to be established to switch the two work modes. Authors in [10, 11] proposed switching the secondary-side compensation structure to obtain constant current and constant voltage. Although the complexity of control is reduced, it increases too many auxiliary switches and circuit cost, and the circuit is still complex because the basic compensation networks of these topologies are double-side LCCLs. Moreover, the compensation networks mentioned above can only be used in full-bridge or half-bridge circuits.

This paper proposes a CL/LCL compensation network that can be used in a single-switch inverter. It can deliver constant current and constant voltage by operating a relay. The structure of the network is simple and the control method is convenient. Finally, it has been proved by theory and experiment that the proposed compensation network can supply constant current and constant voltage when the load changes suddenly.

2. Constant current and constant voltage ICPT topology

2.1. Traditional ICPT topology

A traditional DC/DC ICPT topological circuit first uses a full bridge circuit to realize DC/AC conversion. It generates a high-frequency alternating magnetic field with alternating current in the primary-side coil of a loosely coupled transformer, and then generates induced electromotive force on the secondary-side coil of the loosely coupled transformer to achieve the purpose of energy transmission. As the SP/PP hybrid circuit is shown in Fig. 1, U_{in} is the power supply, C_{in} is the input filter capacitor, and Q_1, Q_2, Q_3 and Q_4 are the switches of a full-bridge circuit. By controlling the on-off of switches Q_5, Q_6 and Q_7, the primary side of the circuit can realize series compensation or parallel compensation. M is the mutual inductance of a loosely coupled transformer. The L_s and C_s are connected in parallel to construct a parallel compensation structure. Finally, they are connected to the load through a rectifier bridge.

The working principle of the circuit is that when the switch Q_6 is turned off, Q_5 and Q_7 are turned on, and the network is the PP structure, which can supply constant current. When
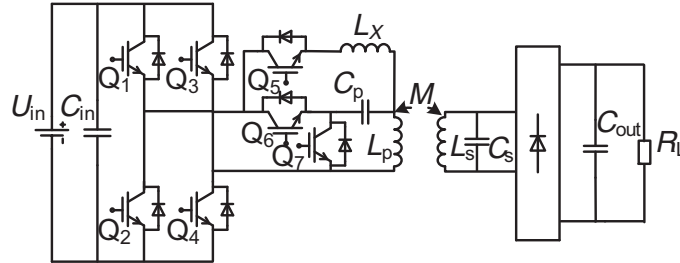
Fig. 1. The hybrid topology circuit of SP/PP

the switches Q_5 and Q_7 are turned off, Q_6 is turned on and the compensation network is the SP structure, which delivers constant voltage.

2.2. The proposed single-switch CL/LCL circuit

A single-switch circuit is developed from a forward converter and a flyback converter [12, 13]. It overcomes the disadvantages that the forward circuit can only transfer power to a secondary-side circuit when the switch is turned on and the flyback circuit can only transfer power to a secondary-side circuit when the switch is turned off. Compared with the full-bridge circuit, the single-switch circuit is simpler and the number of switches is reduced from four to one.

A single-switch CL/LCL circuit is shown in Fig. 2. When the switch Q_1 is turned on, U_{in} transfers power to the secondary side. When the switch Q_1 is turned off, L_p transfers power to the secondary side by resonating with C_p. U_{in} is the power supply of the circuit, C_{in} is the input filter capacitor. The primary-side resonant network consists of C_p and L_p. The secondary-side of the circuit mainly consists of a secondary-side resonant network, a rectifier bridge and a load in parallel. The secondary-side resonant network consists of L_s, C_s, C_1 and L_1. C_{out} is the output filter capacitor. Fig. 3 shows the charging characteristic of a storage battery. I_{cc} is the constant current for the charging battery during the process from 0 to t_1. U_{cc} is the demarcation voltage for switching from the constant current mode to the constant voltage mode. U_{cv} is the constant voltage for charging the battery during the process from t_1 to t_2. The numerical value of U_{cv} is larger than U_{cc}. I_{min} is the minimum cut-off charging current. It can switch the modes between the constant current and constant voltage modes through controlling the switch S. The control flow is shown in Fig. 4, where U_o is the charging voltage and I_o is the charging current.
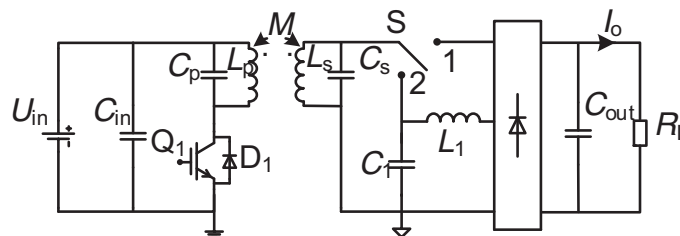

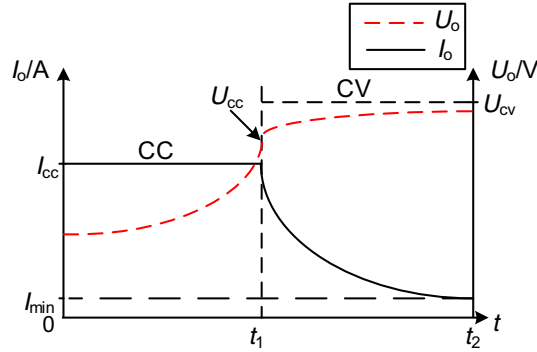Fig. 2. The circuit of single-switch CL/LCL
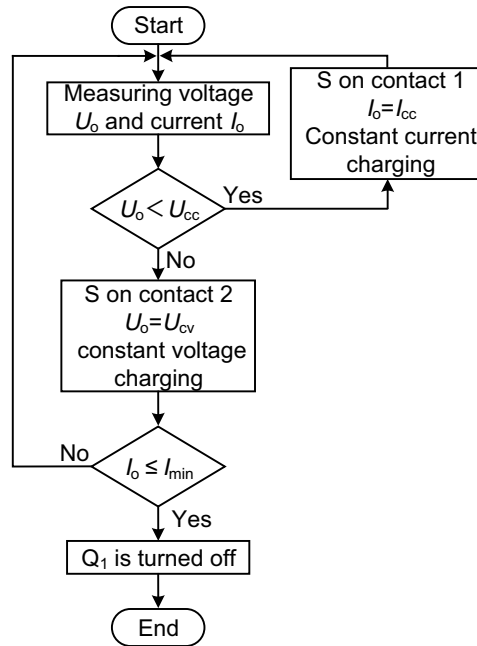
Fig. 3. Charging characteristics of batteries

Fig. 4. The control flow of single-switch CL/LCL circuit

3. Principle analysis and parameter design

3.1. Principle analysis

Firstly, a single-switch CL/LCL circuit is simulated and analysed through Saber software in this paper. The simulation parameters are listed in Table 1 in section 4. The simulation results are shown in Fig. 5. Where U_{gs} is the drive voltage and U_{ds} is the voltage stress on Q_1, and u_{cp} is the voltage on capacitor C_p. Fig. 6 shows the operating process of each mode of the circuit.
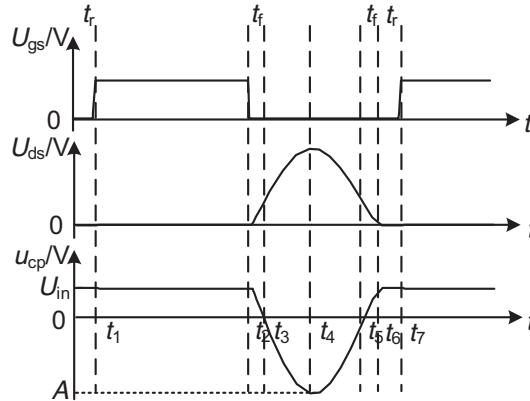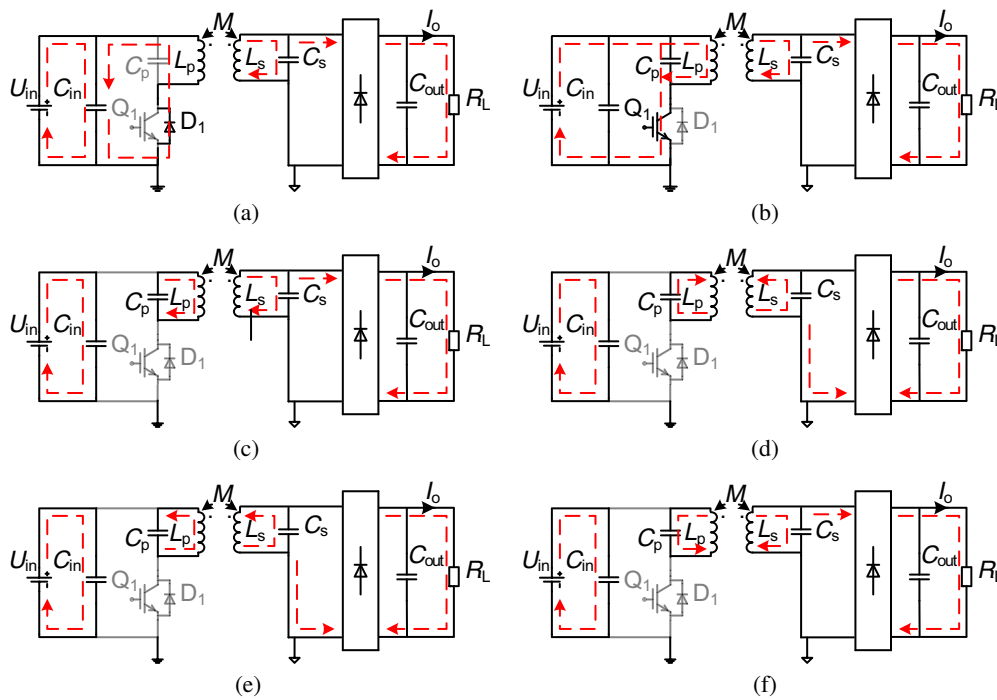
Fig. 5. The simulated waveform of main circuit

Fig. 6. Operating process of main circuit

The process from 0 to t_1, shows the soft switch margin t_r of the switch Q_1. At the zero time, the voltage on the capacitor C_p is equal to U_{in} in numerical value, but in the opposite direction. The voltage on switch Q_1 is zero, and the current on the inductor L_p continues to pass through the parasitic diode D_1 of Q_1. The switch is turned on at this time to creates the zero-voltage switch (ZVS) condition.

During the process from t_1 to t_2, this duration DT is the turn-on time of the switch. At the time t_1, the state of the Q_1 gate is at a high level, and Q_1 realizes the ZVS condition. The voltage on the capacitor C_p is still equal to U_{in}.

During the process from t_2 to t_3, the switch is turned off. The capacitor C_p starts to charge the resonant inductor L_p, and u_{cp} declines to zero at the time t_3.

During the process from t_3 to t_4, the switch is turned off. The inductor L_p is charging the capacitor C_p backward, and u_{cp} is up to the maximum at the time t_4.

During the process from t_4 to t_5, the switch is turned off. The capacitor C_p charges the inductor L_p backward, and u_{cp} declines to zero at the time t_5.

During the process from t_5 to t_6, the switch is turned off and the inductor L_p charges the capacitor C_p forward. u_{cp} increases to the maximum at the time t_6, and it is equal to the power supply voltage U_{in}. The operating cycle is over.

The operating mode during the process from t_6 to t_7 is the same as mode during the process from 0 to t_1. Considering what we have analysed above, it can be seen that the current in the coil L_p changes continuously in one operating cycle, and the power is transferred to the secondary side through the alternating magnetic field.

3.2. Higher harmonic analysis

The mutual inductance equivalent model of the circuit is constructed as shown in Fig. 7. C_p can be regarded as the equivalent voltage source of the circuit, and the voltage on C_p is u_{cp}. Then the mutual inductance equivalent model is transformed into the equivalent model of power supply as shown in Fig. 8.
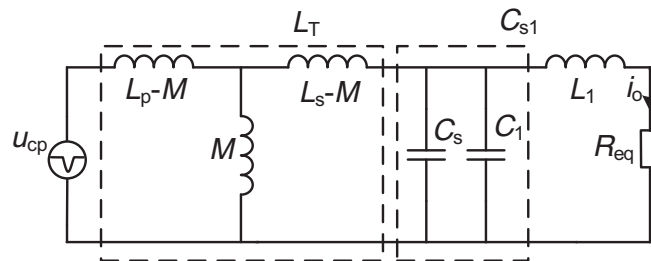

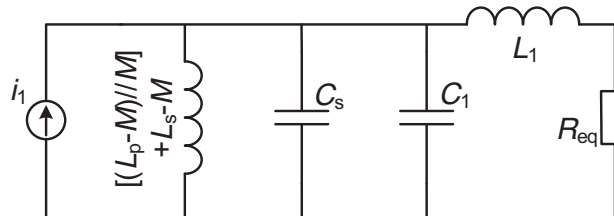Fig. 7. Mutual inductance equivalent model

Fig. 8. The equivalent transformation circuit of power

The current gain of the circuit in constant current mode is calculated. The equivalent inductance of $L_p - M$ in parallel with M and then in series with $L_s - M$ is as follows:

$$j\omega L_T = \frac{j\omega\left(L_p - M\right) \cdot M}{L_p} + j\omega\left(L_p - M\right). \tag{1}$$

The impedance of L_T and C_s are connected in parallel:

$$Z_1 = \frac{j\omega L_T}{1 - \omega^2 L_T \cdot C_s}. \tag{2}$$

The output current in the constant current mode:

$$i_{occ} = \frac{Z_1}{Z_1 + R_{eq}} \cdot \frac{u_{cp} \cdot M}{\omega^2 L_p \cdot L_T}. \tag{3}$$

The current gain of the circuit is:

$$G_{icc} = \frac{i_{occ}}{u_{cp}}. \tag{4}$$

To obtain voltage gain under constant voltage mode based on the constant current mode, the only need is to change the capacitor C_s to C_{s1}. Then the output current i_{ocv} in the constant voltage mode is equal to i_{occ} from (3). The voltage gain of the circuit is:

$$G_{ucv} = \frac{i_{ocv} \cdot R_{eq}}{u_{cp}}. \tag{5}$$

The curves of the current gain in constant current mode and the voltage gain in constant voltage mode are shown in Fig. 9. According to the Saber simulation parameters, when the fundamental frequency is 100 kHz, the maximum current and voltage gains are 0.06 and 0.5, respectively. The current and voltage gains are 3.1×10^{-3} and 0.02, respectively, when the frequency is 200 kHz. The gains under other higher harmonics are lower. It can be seen that the topology has a strong ability to suppress higher harmonics, thus only the fundamental harmonic can be considered.
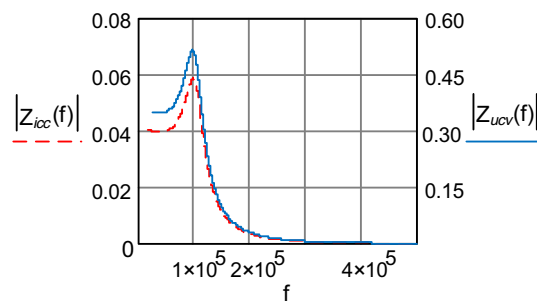

Fig. 9. Current gain of constant current mode and voltage gain of constant voltage mode

According to the analysis of the current and voltage gains of the circuit above, it can be seen that the influence of higher harmonics on the input and output of the circuit can be neglected. We can decompose u_{cp} by Fourier decomposition and get the fundamental wave.

As shown in Fig. 10, the solid line is the waveform of the voltage u_{cp} and the dotted line is the sine wave at the same frequency. u_{cp} can be approximated as a sine wave at the same frequency from the cycle from t_2 to t_6. The voltage of u_{cp} is:

$$\begin{cases} u_{cp} = U_{\text{in}} & (0 - t_2) \\ u_{cp} = A \sin(\omega_1 + \phi) & (t_2 - t_6) \end{cases}. \tag{6}$$
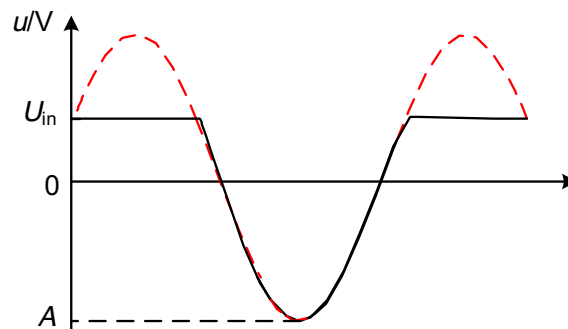

Fig. 10. The fitting chart of u_{cp} and sine wave

When $t_2 < t < t_3$, and $t_5 < t < t_6$, combined with Fig. 5 and (6), we can see that:

$$t_f(A) = \arcsin\left(\frac{u_{cp}}{A}\right)\frac{1}{\omega_1}, \tag{7}$$

where

$$\omega_1(A) = \frac{2\pi}{2 \cdot \left[(1-D)T - 2t_f(A)\right]}. \tag{8}$$

u_{cp} can be simplified in the period of t_2–t_3 and t_5–t_6 from Fig. 5.

$$\int_{t_2}^{t_3} u_{cp} + \int_{t_5}^{t_6} u_{cp} \approx t_f U_{\text{in}}. \tag{9}$$

The equation group of the variable A, which is the amplitude of u_{cp} is as follows:

$$\begin{cases} f(A) = U_{\text{in}}\left[DT + t_f(A)\right] \\ h(A) = \dfrac{A}{\sqrt{2}}\left[(1-D)T - 2t_f(A)\right] \end{cases}. \tag{10}$$

The graph of equation group (10) is shown in Fig. 11. The dotted line refers to the curve of equation $f(A)$, and the solid line is the curve of equation $h(A)$. The voltage at both ends of the capacitance C_p and inductance L_p is equal. According to the principle of volt-second balance, the intersection point of the two lines is the solution of the equation group.
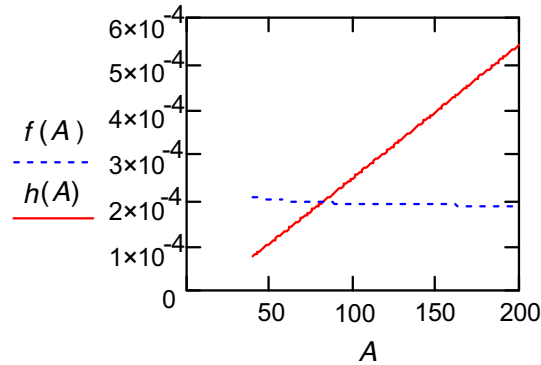
Fig. 11. The diagram of $f(A)$ and $h(A)$

The solutions of the time t_f and the sinusoidal angular frequency ω_1 can be obtained by taking the amplitude A into (7) and (8), respectively. From Fig. 5, we can see that:

$$A \sin (\omega_1 t_3 + \phi) = 0. \tag{11}$$

When ω_1 and t_3 are known, the initial phase ϕ can be calculated by (11). Then u_{cp} is decomposed by Fourier decomposition:

$$a_1 = \frac{2}{T} \int_0^T F(t) \cos(\omega t)\,\mathrm{d}t = \frac{2}{T} \left[\int_0^{t_3} U_{\text{in}} \cos(\omega t)\,\mathrm{d}t + \int_{t_3}^{t_5} A \sin (\omega_1 t + \phi) \cos(\omega t)\,\mathrm{d}t \right], \tag{12}$$

$$b_1 = \frac{2}{T} \int_0^T F(t) \sin(\omega t)\,\mathrm{d}t = \frac{2}{T} \left[\int_{0_3^t} U_{\text{in}} \sin(\omega t)\,\mathrm{d}t + \int_{t_3}^{t_5} A \sin (\omega_1 t + \phi) \sin(\omega t)\,\mathrm{d}t \right], \tag{13}$$

$$d_1 = \sqrt{a_1^2 + b_1^2}, \tag{14}$$

where: d_1 is the amplitude of the u_{cp} fundamental wave and ω is the angular frequency of the fundamental wave. Therefore, the value of u_{cp} can be obtained.

3.3. Parameters calculation

When the circuit is operating in constant current mode at a specific frequency, the resonant capacitor C_s resonates with the inductor L_T. In this case, the expression of i_{occ} is:

$$i_{occ} = \frac{u_{cp} \cdot M}{j\omega \left(L_p \cdot L_s - M^2 \right)}. \tag{15}$$

Before determining the compensation capacitance, the inductances L_p and L_s of the loosely coupled transformer should be determined, and then calculate the mutual inductance M according

to the coupling coefficient. Taking Saber simulation parameters as an example, on the basis of (15), the approximate range of values for L_p and L_s is given, and the coupling coefficient used here is 0.32. A drawing of the three-dimensional graph using the independent variables L_p and L_s, and the dependent variable i_{occ} is shown in Fig. 12, determining the values of inductances L_p and L_s.
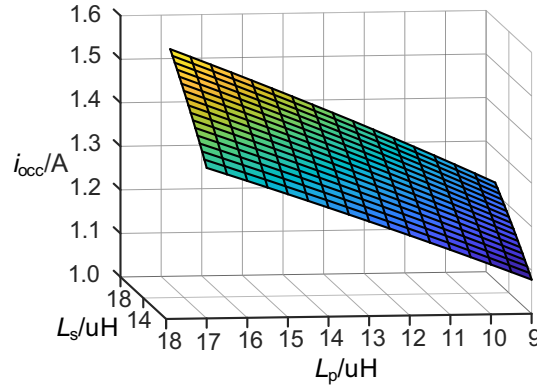

Fig. 12. The diagram i_{occ} varies with L_P and L_S

The capacitor C_s resonates with the inductor L_T, and the value of the capacitor C_s is calculated by (1):

$$C_s = \frac{L_p}{\omega^2 \left(L_p - M\right) \cdot M + \omega^2 \left(L_s - M\right)} \ .$$ (16)

The voltage on the equivalent load R_{eq} in constant voltage mode is u_{ocv}, and the current on the load in constant current mode is i_{ocv}. According to the equivalent exchange of a current source and voltage source, it can be known that:

$$u_{ocv} = \frac{i_{occ}}{j\omega C_1} \ .$$ (17)

The value of the capacitance C_1 can be obtained by (17), and the value of the inductance L_1 can be obtained using the resonance between C_1 and L_1.

To calculate the input impedance of the mutual inductance equivalent model, as shown in Fig. 8, C_p can be regarded as the equivalent input voltage source of the system:

$$\begin{cases} Z_2 = j\omega \left(L_s - M\right) + \dfrac{\dfrac{1}{j\omega C_{s1}} \cdot \left(j\omega L_1 + R_{eq}\right)}{\dfrac{1}{j\omega C_{s1}} + \left(j\omega L_1 + R_{eq}\right)} \\ Z_3 = j\omega \left(L_p - M\right) + \dfrac{j\omega M \cdot Z_2}{j\omega M + Z_2} \end{cases} \ .$$ (18)

In order to realize the ZVS for Q_1, the input impedance Z_{eq} of the whole circuit after parallel connection of C_p and Z_3 should be characterised by low inductivity to make the current lag

voltage at a certain angle in the topology. Turning on the reverse-parallel diode D_1 of Q_1 before the arrival of the high level on the gate causes that the sum of voltage on Z_{eq} and U_{in} is reduced to zero. However, in order to make the whole circuit to operate as close as possible to the zero phase angle, the power factor of the whole system should be considered. Therefore, the selection of C_p should be compromised between these two conditions.

As for the selection of single switch devices, it can be calculated from the principle analysis in section III and the Kirchhoff voltage law that the voltage stresses on Q_1:

$$U_{ds} = U_{in} - u_{cp} . \tag{19}$$

The withstand voltage value of Q_1 must be greater than 1.5 times then the peak value of U_{ds}.

4. Experimental analysis

Based on the detailed analysis of the working principle and parameter design of a single-switch CL/LCL circuit the experimental platform has been constructed, as shown in Fig. 13. Using electronic load as the load of the system, the sudden change of the load can be realized. In the experiment, the vertical distance between the primary-side coil and the secondary-side coil is 40 mm. The other experimental circuit parameters are shown in Table 1.
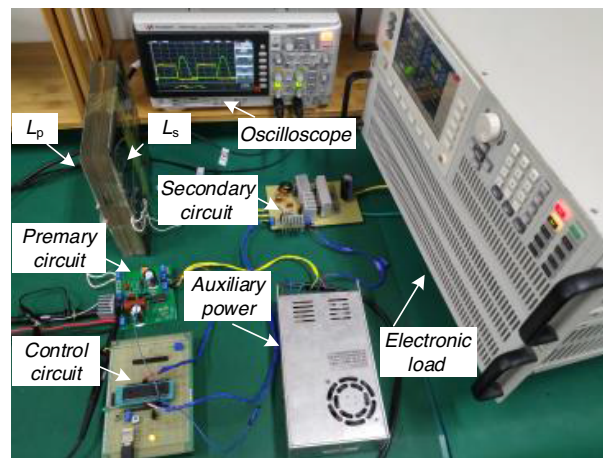

Fig. 13. Experimental platform

Fig. 14 shows the ZVS experimental waveform of the switch Q_1 in the circuit. U_{gs} is the driving voltage waveform between the gate and source of the switch Q_1, and U_{ds} is the voltage waveform between the drain and source of the switch Q_1. The driving voltage U_{gs} of the switch Q_1 is 13 V, and the voltage stress of the switch is 120 V. Before the turn-on pulse arriving, the voltage stress on the switch decreases to 0 V, so the ZVS is realized.

Fig. 15 shows the constant current experimental waveform of the circuit when the switch S is on contact 1. U_{cc} is the voltage on the load and I_{cc} is the current flowing through the load. When

Table 1. Circuit parameters

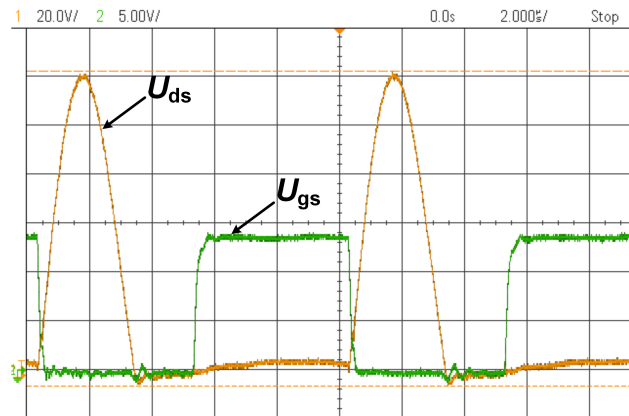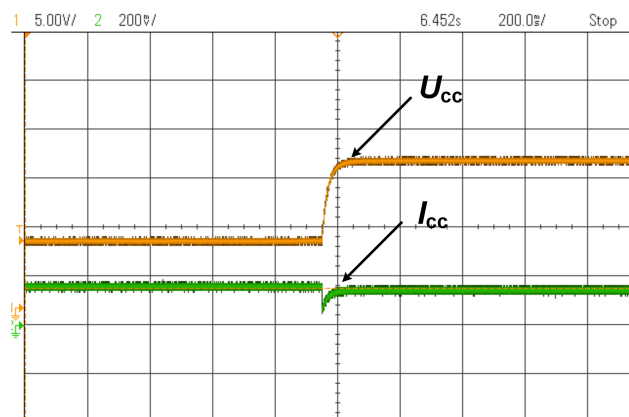| Parameter	Simulation value	Experimental value	Parameter	Simulation value	Experimental value
U_{in}/V	30	30	C_s/nF	180	180
C_{in}/uF	47	47	C_1/nF	180	180
C_p/nF	85	80	L_1/uH	13.3	13.1
L_p/uH	16.8	16.1	C_{out}/uF	47	47
M/uH	5.4	5.2	f_s/kHz	100	100
L_s/uH	17.1	16.5			

Fig. 14. The ZVS waveform of switch Q_1

Fig. 15. The waveform of constant current

the load changes from 5 Ω to 10 Ω, the voltage rises from 7.5 V to 15 V. and there is a small fluctuation of the current, but it recovers to 1.5 A as soon as possible and remains stable.

Fig. 16 shows the experimental waveform of the output voltage and current when the circuit is switched from constant current mode to constant voltage mode. U_{cc} is the voltage on the load in constant current mode. I_{cc} is the current flowing through the load in constant current mode. U_{cv} is the voltage on the load in constant voltage mode. I_{cv} is the current flowing through the load in constant voltage mode. When the switch S is on contact 2, the circuit is switched from constant current mode to constant voltage mode, and the voltage on the load rises by about 1 V and the current rises by about 0.1 A. In other words, the fluctuation rate of the mode switching is about 6.6%.
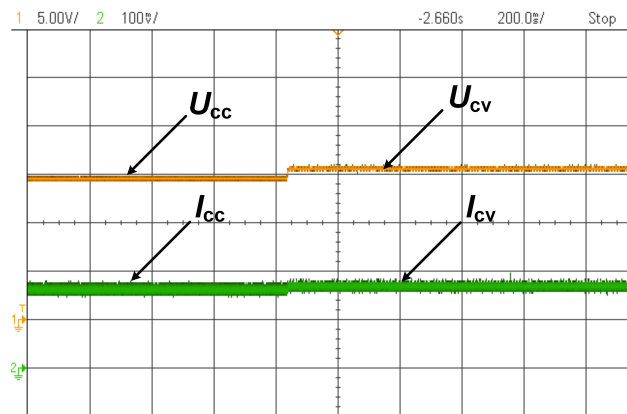

Fig. 16. The waveform of operating mode switching

Fig. 17 shows the constant voltage experimental waveform of the circuit topology when the switch S is on contact 2. U_{cv} is the voltage on the load and I_{cv} is the current flowing through
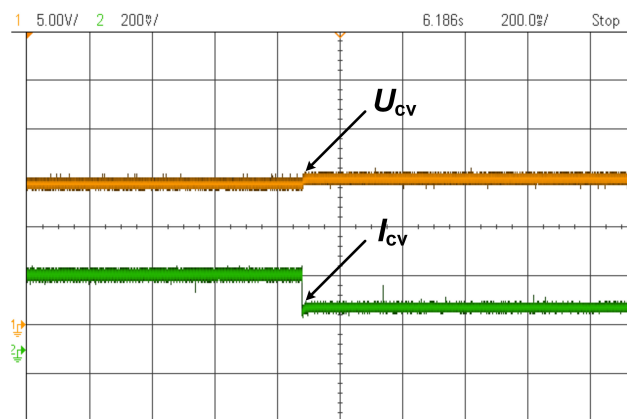

Fig. 17. The waveform of constant voltage

the load. When the load changes from 5 Ω to 10 Ω the current on the load decreases from 3 A to 1.5 A, and the voltage on the load rises slightly, about 0.2 V and about 1.3%. Then it is stable at about 15 V.

5. Conclusion

The traditional circuit of constant current and voltage is analysed briefly, and a single-switch CL/LCL circuit is proposed in this paper. The results of the experiment show that the switch Q_1 of the proposed circuit can realize a ZVS. When the load is changed abruptly, the output voltage is doubled and the fluctuation of the output current is within the allowable range under constant current mode. When the switching is between constant current and constant voltage operating modes, the fluctuations of voltage and current are also within the allowable range. In the constant voltage operating mode, the output current is reduced by two times, and the output voltage fluctuation is also within the allowable range. It can satisfy the constant current charging in the first stage and the constant voltage charging in the second stage. When the battery is charged in the third stage, the circuit works in the constant voltage mode. It can stabilize the charging voltage and reduce the charging current while the battery power is rising continuously until the end of the whole charging process. The circuit has high practical value, due to the simple structure and control method.

References

[1] Prabhat C.G., Pradip K.S., Ankita G. *et al.*, *A new circuit topology using Z-source resonant inverter for high power contactless power transfer applications*, Archives of Electrical Engineering, vol. 66, no. 4, pp. 843–856 (2017).

[2] Liu F., Yang Y., Ding Z. *et al.*, *A Multifrequency Superposition Methodology to Achieve High Efficiency and Targeted Power Distribution for a Multiload MCR WPT System*, IEEE Transactions on Power Electronics, vol. 33, no. 10, pp. 9005–9016 (2018).

[3] Ma G., Jiang L., Chen Y. *et al.*, *Study on the impact of electric vehicle charging load on nodal voltage deviation*, Archives of Electrical Engineering, vol. 66, no. 3, pp. 495–505 (2017).

[4] Zhang H.S., Xiao Y.C., Zhong C.Q., *Modeling of Mutual Inductance Between Superconducting Pancake Coils Used in Wireless Power Transfer (WPT) Systems*, IEEE Transactions on Applied Superconductivity, vol. 29, no. 2, pp. 1–4 (2019).

[5] Dai X., Jiang J., Wu J., *Charging Area Determining and Power Enhancement Method for Multiexcitation Unit Configuration of Wirelessly Dynamic Charging EV System*, IEEE Transactions on Industrial Electronics, vol. 66, no. 5, pp. 4086–4096 (2019).

[6] Li S.Q., Li W.H., Deng J. *et al.*, *A Double-Sided LCC Compensation Network and Its Tuning Method for Wireless Power Transfer*, IEEE Transactions on Vehicular Technology, vol. 64, no. 6, pp. 2261–2273 (2015).

[7] Kan T., Nguyen T., White J.C. *et al.*, *A New Integration Method for an Electric Vehicle Wireless Charging System Using LCC Compensation Topology: Analysis and Design*, IEEE Transactions on Power Electronics, vol. 32, no. 2, pp. 1638–1650 (2017).

[8] Qu X.H., Han H.D., Wong S.C. *et al.*, *Hybrid IPT Topologies With Constant Current or Constant Voltage Output for Battery Charging Applications*, IEEE Transactions on Power Electronics, vol. 30, no. 11, pp. 6329–6337 (2015).

[9] Liu G.J., Bai J.H., Cui Y.L. *et al.*, *Double-Sided LCL Compensation Alteration Based on MCR-WPT Charging System*, Transactions of China Electrotechnical Society, vol. 34, no. 8, pp. 1569–1579 (2019).

[10] Zhang H., Wang H.M., Li N. *et al.*, *Analysis on Hybrid Compensation Topology Circuit for Wireless Charging of Electric Vehicles*, Automation of Electric Power Systems, vol. 40, no. 16, pp. 371–75 (2016).

[11] Ji L., Wang L.F., Liao C.L. *et al.*, *Research and Design of Automatic Alteration between Constant Current Mode and Constant Voltage Mode at the Secondary Side Based on LCL Compensation Network in Wireless Power Tranfer Systems*, Transactions of China Electrotechnical Society, vol. 33, sup. 1, pp. 38–44 (2018).

[12] Kawa A., Penczek A., Pirog S., *DC-DC boost-flyback converter functioning as input stage for one phase low power grid-connected inverter*, Archives of Electrical Engineering, vol. 63, no. 3, pp. 393–407 (2014).

[13] Liu S., Wang B., *Design of quasi-resonant flyback secondary intrinsically safe power supply*, Archives of Electrical Engineering, vol. 68, no. 1, pp. 5–13 (2019).